

Cite this: *Nanoscale*, 2015, **7**, 12955

Solvothermal synthesis and controlled self-assembly of monodisperse titanium-based perovskite colloidal nanocrystals†

Daniela Caruntu,^{a,b} Taha Rostamzadeh,^c Tommaso Costanzo,^{a,b} Saman Salemizadeh Parizi^{a,b} and Gabriel Caruntu^{*a,b}

The rational design of monodisperse ferroelectric nanocrystals with controlled size and shape and their organization into hierarchical structures has been a critical step for understanding the polar ordering in nanoscale ferroelectrics, as well as the design of nanocrystal-based functional materials which harness the properties of individual nanoparticles and the collective interactions between them. We report here on the synthesis and self-assembly of aggregate-free, single-crystalline titanium-based perovskite nanoparticles with controlled morphology and surface composition by using a simple, easily scalable and highly versatile colloidal route. Single-crystalline, non-aggregated BaTiO₃ colloidal nanocrystals, used as a model system, have been prepared under solvothermal conditions at temperatures as low as 180 °C. The shape of the nanocrystals was tuned from spheroidal to cubic upon changing the polarity of the solvent, whereas their size was varied from 16 to 30 nm for spheres and 5 to 78 nm for cubes by changing the concentration of the precursors and the reaction time, respectively. The hydrophobic, oleic acid-passivated nanoparticles exhibit very good solubility in non-polar solvents and can be rendered dispersible in polar solvents by a simple process involving the oxidative cleavage of the double bond upon treating the nanopowders with the Lemieux–von Rudloff reagent. Lattice dynamic analysis indicated that regardless of their size, BaTiO₃ nanocrystals present local disorder within the perovskite unit cell, associated with the existence of polar ordering. We also demonstrate for the first time that, in addition to being used for fabricating large area, crack-free, highly uniform films, BaTiO₃ nanocubes can serve as building blocks for the design of 2D and 3D mesoscale structures, such as superlattices and superparticles. Interestingly, the type of superlattice structure (simple cubic or face centered cubic) appears to be determined by the type of solvent in which the nanocrystals were dispersed. This approach provides an excellent platform for the synthesis of other titanium-based perovskite colloidal nanocrystals with controlled chemical composition, surface structure and morphology and for their assembly into complex architectures, therefore opening the door for the design of novel mesoscale functional materials/nanocomposites with potential applications in energy conversion, data storage and the biomedical field.

Received 1st February 2015,
Accepted 7th June 2015

DOI: 10.1039/c5nr00737b
www.rsc.org/nanoscale

1. Introduction

Titanium-based perovskite oxides have attracted considerable attention in the past decade due to their unique physical and chemical properties which can be used in cutting-edge applications such as data storage,¹ water splitting,² energy conversion and storage,³ solid oxide fuel cells,⁴ multiferroics,⁵ spintronics⁶ and photovoltaics.⁷ Among titanium-containing perovskites BaTiO₃ is the only ferroelectric material with a Curie point, *i.e.* the temperature at which the paraelectric–ferroelectric transition occurs, very close to room temperature ($T_c = 120$ °C). Since the ferroelectric properties of materials scale with the size of the grains and the dielectric permittivity of a ferroelectric is maximum in the vicinity of the ferroelec-

^aDepartment of Chemistry and Biochemistry, Central Michigan University, 1200, S. Franklin St., Mt. Pleasant, MI 48858, USA

^bScience of Advanced Materials (SAM) Program, Central Michigan University, 1200, S. Franklin St., Mt. Pleasant, MI 48858, USA. E-mail: g.caruntu@cmich.edu; Fax: +1-(989)-774-3883; Tel: +1-(989)-774-3863

^cChemistry Department, University of New Orleans, New Orleans, LA 70148, USA

† Electronic supplementary information (ESI) available: FE-SEM image of 12 nm BaTiO₃ nanocubes deposited onto a silicon wafer (Fig. SI1), the X-ray diffraction pattern of a superlattice structure formed by monodisperse 10 nm BaTiO₃ cuboidal nanocrystals (Fig. SI2) and TEM images of a BaTiO₃ superparticle (Fig. SI3). See DOI: 10.1039/c5nr00737b

tric-paraelectric phase transition, its relatively low Curie temperature makes BaTiO₃ the premier material for the design of high-*k* polymer-ceramic nanocomposite films for flexible capacitors in energy storage applications.^{11,14–17} From a structural point of view, the ferroelectric order is triggered in titanium-containing perovskites by the off-center shift of the Ti⁴⁺ ions within the unit cell. In turn, this leads to the formation of dielectric dipoles and the onset of an intrinsic lattice polarization accompanied by the lowering of the symmetry of the unit cell from cubic (S. G. Pm3m) to tetragonal (S. G. P4mm). In addition to the formation of electrical dipoles and the polar ordering, non-centrosymmetric BaTiO₃ crystals possess unique non-linear optical properties, such as the second harmonic generation (SHG) effect. Specifically, when non-centrosymmetric BaTiO₃ crystals are excited with a fundamental frequency they emit optical signals at a frequency which is double the fundamental excitation frequency. Recent research suggested that the second harmonic generation (SHG) effect can be exploited for the design of frequency doublers in lasers, as well as probes in the study of surface chemistry.⁸ Moreover, non-centrosymmetric nanocrystals can be used as probes in early cancer detection⁹ and *in vivo* cellular imaging¹⁰ because they can provide an effective mechanism of contrast and separation between the excitation wavelength and the signal generated by the markers. In addition, the coherent and non-saturating signal and the flexibility in selecting the excitation wavelength will alleviate the long-standing problems of bleaching, dye saturation and blinking associated with the use of conventional fluorescent dyes, quantum dots or green fluorescent proteins, thereby promising a substantial improvement of the existing imaging techniques. For both fundamental studies, such as the investigation of the survival of the ferroelectric order and the polarization structure in nanoscale systems and the implementation of nanoscale titanium-containing perovskites in practical applications there is a stringent need for aggregate-free dielectric and/or ferroelectric ceramic nanoparticles with controllable size, shape and surface composition. It is well-known that the structural, dielectric, ferroelectric and thermodynamic properties of perovskites vary dramatically with the grain size.¹¹ For example, the dielectric permittivity of 10 μm BaTiO₃ grains is about 1500–2000 and peaks at a value $\epsilon_r = 5000$ when the size decreases to 1 μm followed by a steep decrease when the grain size reaches the nanometer-length scale.^{11b}

Despite a decade of intense research the question whether or not ferroelectricity survives in low-dimensional perovskites still remains elusive and therefore, the values of the critical size at which the ferroelectricity would be suppressed range typically between 4 and 120 nm.¹² Due to their size and shape uniformity, single-domain titanium-containing perovskite nanoparticles are attractive for the design of novel ferroelectric metamaterials *via* self-assembly into 2D and 3D periodic arrangements. These include nanocrystal-based freestanding ultrathin membranes,¹³ superlattices,¹⁴ superparticles¹⁵ supracrystals,¹⁶ as well as binary superlattices,¹⁷ whereby the ferroelectric nanocrystals can be combined with semiconducting,

metallic or magnetic nanocrystals with similar sizes and shapes *via* a modular approach. Such hierarchically complex structures are expected to exhibit a rich structural diversity and, therefore possess novel physical properties originating from both the properties of individual colloidal nanocrystals and the mutual interactions between them which can be exploited in the design of novel functional devices.¹⁸ Although many synthetic sol-gel routes have been proposed for the fabrication of titanium-containing perovskite fine powders, most of them rely on the hydrolysis and condensation of titanium alkoxide precursors in aqueous solutions containing stoichiometric amounts of alkaline-earth ions. Such reactions can be performed either at room temperature¹⁹ or can be accompanied by a high temperature/hydrothermal treatment in which the reaction intermediates are converted into highly crystalline perovskite phases.²⁰ It is well-known that M(OR)₄ alkoxides (M = Ti, Zr) possess a high reactivity towards hydrolysis and the nucleophilic attack of the water molecules to the highly charged Lewis acidic M⁴⁺ centers is fast, thereby leading to the spontaneous precipitation of metal hydroxides. Consequently, this enables a very little control over the nucleation and growth processes, as well as the structural evolution of the oxide, which results in most cases into aggregated, irregularly-shaped polydisperse perovskite nanoparticles. To alleviate this problem and improve the control over the size and shape of the nanoparticles, different groups developed non-hydrolytic routes for the synthesis of nanoscale perovskites, including the thermal decomposition of barium titanium glycolates,²¹ titanium butoxide oleates,²² the *in situ* growth of nanoparticles from a Ti-containing intermediate²³ or the reaction of alkaline-earth metal ions with the corresponding metal alkoxides in non-aqueous solutions.²⁴ However, in most cases the reaction steps are complicated and use hazardous precursors along with a limited control over the morphology of the perovskite nanocrystals.

Recently, our group proposed a novel synthetic approach for the synthesis of aggregate-free cube like BaTiO₃ colloidal nanoparticles by using a simple phase transfer process at temperatures as low as 135 °C²⁵ and demonstrated that ferroelectricity survives in non-interacting nanocrystals of a size down to 5 nm at room temperature.²⁶ In this paper we show that the rational control of the reaction conditions allows for the synthesis of deagglomerated and nearly monodisperse titanium-containing perovskite colloidal nanocrystals with controlled chemical composition and morphology. By using BaTiO₃, an archetypal ferroelectric titanium-containing perovskite, as a model system, we demonstrate that the shape of the nanocrystals can be varied from spheroidal to cubic by tuning the polarity of the solvent and their size can be controlled in a wide range by adjusting the concentration of the precursors and the reaction temperature, respectively. We also demonstrate that the surface composition of the nanocrystals can be tuned *via* simple ligand-exchange and/or chemical reactions and the as-prepared, hydrophobic, nanoparticles can be rendered hydrophilic, which can potentially make them attractive for various applications in the biomedical field. Last, but not

least, we demonstrate for the first time that due to the shape and size uniformity of the ferroelectric nanocubes they can assemble into complex hierarchical 2D and 3D structures such as monolayers, superlattice assemblies and superparticles, which can be interesting systems for the study of the collective properties of ferroelectric nanocrystals. Also, we show that the proposed synthetic methodology can be extended to the preparation of other nanoscale titanium-containing perovskite electroceramics, which will open the door to a systematic study on the influence of the chemical composition, nanoparticle size and surface curvature on the polar ordering in nanoscale ferroelectric materials.

2. Experimental

2.1. Synthesis of perovskite colloidal nanocrystal nanoparticles

Analytical grade reagents, including metal nitrates $\text{Ba}(\text{NO}_3)_2$, $\text{Pb}(\text{NO}_3)_2$, titanium butoxide ($[\text{Ti}(\text{OBu})_4]$ 97%), and $\text{Zr}(\text{OBu})_4$ in 1-butanol, ethanol, 1-butanol, 1-decanol, NaOH , and oleic acid (OA 90% technical grade) were purchased from Alfa Aesar and used without any further purification. In a typical synthesis for the preparation of BaTiO_3 nanocrystals, two aqueous solutions containing 1 mmol $\text{Ba}(\text{NO}_3)_2$ and 12.5 mmol NaOH were mixed with a 1-BuOH solution containing 1 mmol of $\text{Ti}(\text{Bu})_4$ and 2.5 mL of oleic acid in BuOH resulting in a white creamy solution which was stirred vigorously for 5 min. The resulting mixture was subsequently transferred to a 23 mL Teflon-liner and then placed into a stainless steel autoclave (Parr Instruments). The autoclave was sealed and the reaction mixture was heated to 180 °C and maintained at this temperature for 18 h. At the end of the reaction the autoclave was cooled naturally to room temperature and the resulted powders were separated by centrifugation. The nanocrystals were then collected, washed with ethanol several times and then dispersed in non-polar solvents (toluene, heptane, etc.) yielding stable colloidal solutions. The typical yield of the perovskite nanoparticles was 85–90%.

2.2. Nanoparticle self-assemblies, single-component superlattice structures and superparticles

The resulting colloidal nanocrystals can be assembled into monolayers by casting several drops of a toluene solution (5–10 mg mL⁻¹ nanoparticles) onto Formvar carbon films on 200 mesh copper grids followed by the natural evaporation of the solvent at room temperature. More complex hierarchical nanostructures, such as superlattice assemblies and superparticles, can be obtained from uniformly-sized perovskite colloidal nanocrystals by placing a substrate (copper grids or silicon substrates) at the bottom of a vial containing a toluene solution of nanocrystals and allowing the solvent to evaporate naturally at room temperature.

2.3. Surface modification of BaTiO_3 colloidal nanocrystals

For ligand-exchange reactions 25 mg of BaTiO_3 nanopowder containing 15 nm oleic acid-capped nanocubes was dissolved

in 5 mL hexane and the resulting solution was mixed with 5 mL of *N,N*-dimethylformamide containing 0.05 mmol NOBF_4 . The resulting mixture was gently shaken for several minutes until the nanocrystals passed from the non-polar to the polar phase. At the end of the process the hexane phase was removed with a pipette and the DMF solution of BaTiO_3 nanocrystals was recovered and stored for several months at room temperature. The oxidation reaction was performed by treating 100 mg of oleic acid-capped 15 nm BaTiO_3 nanocubes dispersed in 20 mL cyclohexane with 20 mL solution of Lemieux-von Rudloff reagent (0.105 mM KIO_4 and 5.7 mM KMnO_4) in the presence of K_2CO_3 and *tert*-butanol. The resulting mixture was stirred vigorously at 40 °C for 48 h and at the end of the reaction the product was washed to remove the bi-products and centrifuged under conditions similar to those described by Chen and coworkers.²⁷

2.3.1. Characterization. (a) **Transmission electron microscopy (TEM) and elemental analysis by energy-dispersive X-ray spectroscopy (EDX).** The morphology, phase purity and crystallinity of the BaTiO_3 nanoparticles were investigated by transmission electron microscopy (TEM), HRTEM, EDX and SAED with a JEOL 2200FS microscope with a resolution of 0.19 nm at a bias voltage of 200 kV and a FE-SEM (JEOL 7500F). For electron microscopy experiments, several drops of BaTiO_3 nanocrystal-containing solutions were cast under ambient conditions onto carbon-coated copper TEM grids. The average size of the nanoparticles was estimated by averaging the size of about 100 nanoparticles from the corresponding TEM micrographs. (b) **Powder X-ray diffraction.** The phase purity and the crystal structure of the nanopowders were studied by powder X-ray diffraction (XRD) with a Panalytical X'Pert system using monochromatic Cu K_α radiation ($\lambda = 1.54056 \text{ \AA}$ at 40 kV and 40 mA). Diffraction data were collected at room temperature by step scanning in the range $15^\circ \leq 2\theta \leq 75^\circ$ with a step size of 0.02° and a time per step of 10 s and the collected data were analyzed using the X'Pert High score software. The size of the crystallites was determined by the analysis of the three most intense peaks in the corresponding XRD patterns by the Scherrer method using silicon as a standard.

(c) **Fourier transform infrared (FT-IR) spectroscopy.** The surface composition of the BaTiO_3 nanoparticles was studied with a Thermo Nicolet Omnic FT-IR spectrometer in the attenuated total reflection mode and the wavelength range varied from 500 to 4000 cm⁻¹. (d) **Raman spectroscopy.** Raman spectra were recorded with a Horiba Jobin Yvon Xplora Raman Spectrometer using a 100× microscope objective and a 532 nm excitation of an Nd/YAG laser with a maximum power of 15 mW. The measurements were performed with a 10 μm pinhole and a spectral resolution of 1 cm⁻¹. The laser spot size was 2 μm and the collected data were analyzed with Labview 6 software provided by Horiba in order to precisely locate the Raman bands. (e) **Thermal analysis.** Thermal analysis (TA) and differential scanning calorimetry measurements were performed in the temperature range from 25 to 600 °C using a TA SDT-Q600 instrument under a flowing N_2 atmosphere with a scan speed of 2° min⁻¹ in the heating step and 5° min⁻¹ in the cooling step, respectively.

3. Results and discussion

3.1. Formation of the perovskite colloidal nanocrystals

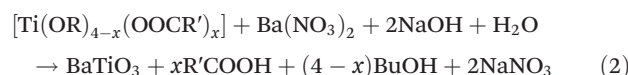
The hydrolysis of $M(OR)_4$ ($M = Ti, Zr$) alkoxide precursors has been long investigated in order to understand the mechanism of nanoscale oxide formation and identify the factors that control the size and shape of the constituting particles, their internal structure and porosity. Highly charged transition metal M^{4+} ions, such as Ti or Zr are very susceptible to the nucleophilic attack of water molecules when coordinated to highly electronegative species, such as alkyl groups. This generally favors rapid hydrolysis-condensation/polymerization reactions leading to the uncontrolled branching of the $M-O-M$ networks and the formation of precipitates rather than gels.²⁸ Depending upon the pH of the solution, the hydrolysis of titanium alkoxides has been conventionally described by two different mechanisms. In basic solutions it involves a classical SN_2 -type reaction consisting of the nucleophilic addition of HO^- species to positively charged M^{4+} ions and the release of the alkoxide ion. Likewise, in acidic solutions one oxygen atom in the alkoxide group is protonated with the release of an alcohol molecule followed by the regeneration of the protons in acidic solutions (SN_1). The hydrolysis is generally accelerated by the presence of high amounts of water which yields amorphous precipitates consisting of big aggregated particles with less defined sizes and shapes which can be converted into the metal oxides by a subsequent thermal treatment. Several strategies, involving the formation of thermodynamically stable complexes *via* the chemical modification of the alkoxide precursors with different compounds, such as amines,²⁹ alkoxy- and aminoalcohols,³⁰ oximes,³¹ β -diketones,^{30b,32} β -ketoesters³³ or carboxylic and phosphonic acids³⁴ have been proposed.

These will not only increase the stability of the alkoxides, but will also hinder the nucleophilic attack of HO^- ions to the metal centers eventually slowing down the hydrolysis rate of the M^{4+} ions ($M = Ti, Zr$). Cozzoli *et al.* showed that the treatment of Ti alkoxides with long chain carboxylic acids yields polynuclear oxocarboxyalkoxides in which hexacoordinated Ti^{4+} ions are surrounded by bulky carboxylate ligands. As a result, the ligands provide an effective steric hindrance to the Lewis acidic centers, thereby making very difficult the nucleophilic attack of water molecules and preventing the spontaneous precipitation of amorphous TiO_2 .^{34b} It has been suggested that the cross-linking of the $Ti-O$ bonds is controlled by the amount of water in the system. Thus, when a large volume of water was injected into the system the hydrolysis reaction occurred quickly facilitating the anisotropic growth of nanostructures and leading to the formation of TiO_2 nanorods. Conversely, when the amount of water in the system was low, the hydrolysis occurred slowly leading to an isotropic growth of the nanostructures and the formation of spheroidal TiO_2 nanoparticles. In line with these experimental observations, the synthesis of perovskite colloidal nanoparticles was performed in microemulsions containing transition metal alkoxyl carboxylates generated *in situ* from the reaction between

$M(OBu)_4$ ($M = Ti, Zr$) and oleic acid, as evidenced by the color change of the reaction mixture from colorless to faint yellow when the precursor solutions were mixed together:



In such conditions, we hypothesize that oxide nanoparticles nucleate and grow under solvothermal conditions in a microemulsion formed by mixing the aqueous phase with the oil phase as a result of the reaction between Ba^{2+} ions and the titanium alkoxyl carboxylates according to the following reaction:



In addition to deprotonating the oleic acid molecules the OH^- ions are believed to exert a catalytic effect by favoring the conversion of the $Ba-OH$ bonds into crystalline $BaTiO_3$.³⁵

3.2. Synthesis of size controlled perovskite nanocubes

As seen from the TEM images presented in Fig. 1a and b, $BaTiO_3$ nanocubes obtained from mixtures of 1-butanol and 1-decanol are nearly monodisperse and present an average edge length of 10 ± 1 nm. The nanoparticles are well-separated due to the attachment of oleic acid molecules on the surface of each individual nanocrystal which enables them to organize on planar surfaces with the formation of self-assembled monolayers. The HRTEM image of an individual 10 nm $BaTiO_3$ nanocube (Fig. 1c) reveals a uniform contrast across the nanoparticle indicating a high crystallinity, despite the relatively low reaction temperature. The lattice fringes observed by HRTEM correspond to an interplanar distance of 4.09 Å, ascribed to the {001} family of planes. Preliminary studies suggested that several reaction parameters, including the con-

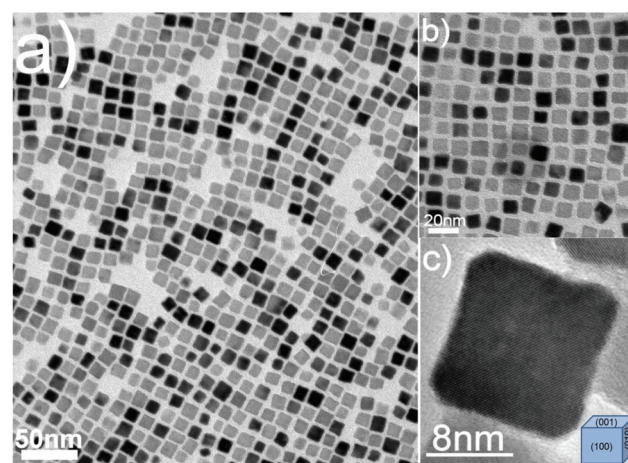


Fig. 1 TEM images (a, b) of self-assembled monolayers of 10 nm $BaTiO_3$ nanocubes obtained under solvothermal treatment of a solution containing 1 mmol of $Ba(NO_3)_2$ and 1 mmol of $Ti(OBu)_4$ at 180 °C for 48 h; (c) high resolution TEM (HRTEM) image of an individual 10 nm $BaTiO_3$ nanocube.

centration of the precursor, the nature of the solvent and the reaction time play a significant role on the morphology of the BaTiO₃ nanocrystals. Table 1 summarizes the morphology and average size of the BaTiO₃ nanocrystals obtained from mixtures in which 1-decanol has been replaced with other solvents with different polarities. Fig. 2 shows the TEM images of BaTiO₃ colloidal nanocrystals obtained under the same conditions as those used in the preparation of 10 nm nanocubes (see the Experimental section) except for 1-decanol, which has been replaced by various other solvents. As seen in the TEM images, BaTiO₃ nanocrystals obtained from solutions containing benzyl alcohol (BA), diethylene glycol (DEG) and diethylene glycol monobutyl ether (DEGMME) are quasi-spheroidal with an average diameter of 32, 18, and 16 nm, respectively whereas nanocrystals obtained from toluene (TOL), phenyl ether (PE) and benzyl ether (BE) are cubic with an average edge length of

10, 10 and 8 nm, respectively. The nanoparticles are also well separated and have the tendency to arrange into monolayers on planar surfaces, such as the microscope grid. Based on the small-angle (SAXS) and wide-angle X-ray scattering (WAXS) study, Hu and coworkers suggested recently that the type of microemulsion formed by the precursors in the solvothermal synthesis of perovskite nanoparticles plays a key role in the morphology of the nanoparticles.³⁶ Specifically, oleic acid and oleate ions form predominantly lamellar micelles stabilizing cuboidal nanocrystals.

By varying the concentration of the fatty acid in solution, the lamellar structure of the micellar architectures is altered with the stabilization of normal/reverse micelles, thereby favoring the formation of nanocrystals with irregular round-shape or nanorod-type morphology. More recently, Friderichs *et al.* presumed that at the oil–water interfaces of two-phase mixtures the metal fatty acid salts adopt a nematic liquid crystal structure. Such structures depend on the type of base added to the solution and seem to play an important role on the morphology of perovskite nanocrystals prepared under solvothermal conditions.³⁷ Although we do not completely rule out the influence of the type of micellar solutions on the morphology of the perovskite nanocrystals our preliminary experiments strongly suggest that the polarity of the solvent is also an important parameter in the growth mechanism of the perovskite nanoparticles. Specifically, while the addition of organic solvents with a relatively high dielectric constant, such as diols and benzyl alcohol leads to the stabilization of spheroidal BaTiO₃ nanocrystals ($\epsilon_{\text{DEG}} = 32$; $\epsilon_{\text{BA}} = 13.1$ and $\epsilon_{\text{DEGMME}} = 12.6$, respectively) the cubic shape, characterized by low energy (001)

Table 1 Morphology of the BaTiO₃ colloidal nanocrystals as a function of the composition of the solvent

Composition of the solvent	Morphology	Particle size (nm)
1-Butanol-benzyl alcohol	Spheroidal	30 ± 4
1-Butanol-diethylene glycol	Spheroidal	18 ± 3
1-Butanol-diethylene glycol monobutyl ether	Spheroidal	15 ± 3
1-Butanol-toluene	Cuboidal	9 ± 2
1-Butanol-phenyl ether	Cuboidal	10 ± 2
1-Butanol-benzyl ether	Cuboidal	9 ± 1

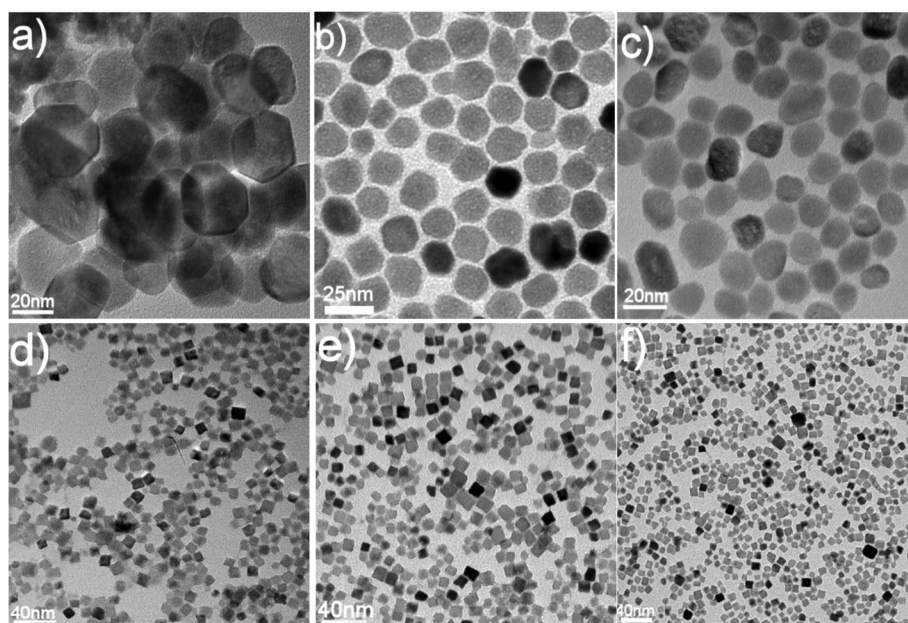


Fig. 2 TEM images (a, b) of BaTiO₃ nanoparticles obtained under a solvothermal treatment from mixtures of 1-butanol and a second solvent (1 : 1 volume ratio): (a) benzyl alcohol; (b) diethylene glycol (DEG); (c) diethylene glycol monobutyl ether; (d) toluene; (e) phenyl ether and (f) benzyl ether.

terminal planes is stabilized in solvents with lower values of the dielectric constant ($\epsilon_{\text{PE}} = 3.9$; $\epsilon_{\text{BE}} = 3.86$ and $\epsilon_{\text{TOL}} = 2.4$, respectively). In addition to the polarity of the solvent the sodium oleate formed *in situ* from the deprotonation of oleic acid molecules by NaOH could play a role in the stabilization of the cubic shape. Wu and coworkers suggested recently that sodium oleate binds preferentially to the {001} planes of oxides, thereby promoting a faster growth along the <111> directions and stabilizing the cuboidal shape of transition metal ferrite nanocrystals.³⁸ Experiments aimed at understanding the role of the polarity of the solvent on the morphology of BaTiO₃ nanocrystals obtained by this route are currently underway and will be reported in a forthcoming paper.

Preliminary results showed that the concentration of the salt precursors play a major role in controlling the size of the BaTiO₃ nanocubes. Fig. 3 shows the TEM micrographs of BaTiO₃ nanoparticles obtained from solutions in which the concentration of the Ba(NO₃)₂ and Ti(OBu)₄ varied from 2 mM to 1.5, 1, 0.85, 0.75 and 0.5 mM, while maintaining the concentration of the base and the alcohol constant. Examination of the TEM micrographs revealed that after a solvothermal treatment at 180 °C for 48 h the size of the resulting colloidal BaTiO₃ nanocubes varied from 5, 8, 10, 12, 15 to 20 nm, respectively. The statistical particle size distribution of the nanocubes was less than 5%, thereby indicating that the nanocrystals are nearly monodisperse. A similar trend in the variation of the size of BaTiO₃ nanoparticles obtained by coprecipitation or hydrothermal treatment was observed by other groups³⁹ and the increase in the size of the nanocubes with decreasing concentration of the precursors in solution can be

reasonably explained in terms of the LaMer model of nanoparticle growth.⁴⁰ According to this model, the formation of nanocrystals in solution is conventionally described as occurring through a short burst of nucleation followed by the growth of the resulting nuclei. When the initial concentration of the precursors in a solution is high the solution becomes quickly supersaturated leading to a large number of nuclei. In such a case the nucleation process dominates the crystal growth, thereby yielding small BaTiO₃ nanocrystals. Conversely, a low concentration of the precursors in solution will drastically limit the number of nuclei which form in the initial stage of the reaction. In such a case the concentration of the monomer in solution is still high after the nucleation process and the diffusion-mediated growth process is dominant, thereby leading to the formation of larger nanoparticles. It is worth noting that the reaction time was also found to play an important role in the control of the size of BaTiO₃ nanocrystals. Fig. 4 shows the TEM micrographs of BaTiO₃ cuboidal nanocrystals obtained after a solvothermal treatment of the solution at 180 °C for 72, 96 and 120 h, respectively. Nanocubes are nearly monodisperse, possess well-defined faces and are well-separated. Moreover, their average edge length increased from 40 ± 2 to 50 ± 1 and 78 ± 2 nm when the reaction time varied from 72 to 120 h. A closer examination of the TEM images also reveals that the big nanocrystals have the tendency to form extended 2D-superstructures and they coexist with a small population of smaller cuboidal nanocrystals with an average size of 10 nm. It is also worth noting that the distances between the nanocubes are about 2.7 nm, a value which is much reduced compared to the double value of the chain length of the oleic acid molecule (~1.8 nm). This indicates

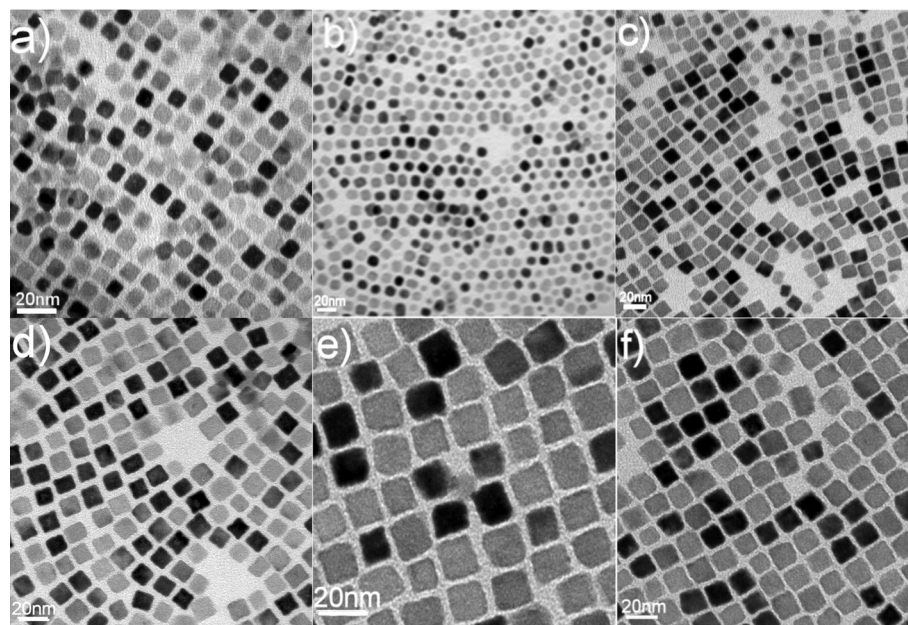


Fig. 3 TEM micrographs of variable-size BaTiO₃ cuboidal nanocrystals: 5 nm (a), 8 nm (b), 10 nm (c), 12 nm (d), 15 nm (e), 20 nm (f) obtained by varying the concentration of the precursors.

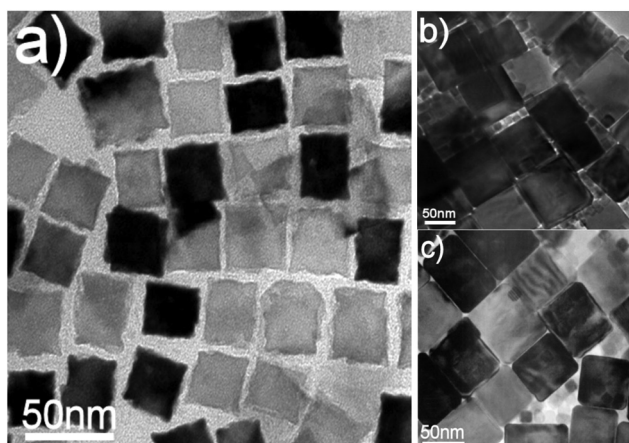


Fig. 4 TEM micrographs of BaTiO_3 nanocubes obtained at $180\text{ }^\circ\text{C}$ after a reaction time of 72 (a), 96 (c) and 120 hours (c), respectively.

that the oleic acid molecules attached to the surface of adjacent nanoparticles are not connected in an end-to-end fashion, but they rather penetrate into the ligand chains of the neighboring nanocrystals, thereby suggesting the existence of strong ligand-ligand interactions in these nanostructures.

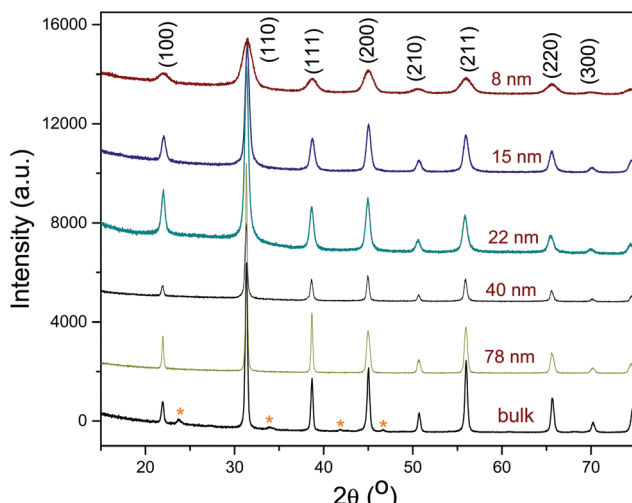


Fig. 5 Powder X-ray diffraction patterns of variable-size BaTiO_3 nanocubes obtained at $180\text{ }^\circ\text{C}$ compared with the pattern of the commercial bulk BaTiO_3 (bottom pattern). The peaks marked with a red star in the pattern of the bulk BaTiO_3 correspond to BaCO_3 (PDF no. 14-0373).

3.3. Crystal structure of variable-sized BaTiO_3 nanopowders

The composition and phase purity of variable-sized BaTiO_3 nanocrystals were studied by conventional X-ray powder diffraction. As seen in Fig. 5, the nanopowders are well-crystallized, despite the relatively low temperature at which the solvothermal treatment was carried out and are free of impurities, such as BaCO_3 which has been observed in the commercial bulk BaTiO_3 sample. It is worth mentioning that the sole analysis of the XRD patterns is not conclusive as to whether a tetragonal distortion is present or not in these nanopowders. This is because the splitting of the (200) peak around 45° in 2θ , commonly ascribed to an off-center shift of the Ti^{4+} ions within the TiO_6 octahedra forming the perovskite structure is obscured by a peak broadening effect associated with the small size of the crystallites. However, as we demonstrated recently, BaTiO_3 nanocubes with an average edge-length down to 5 nm exhibit, at least at the local scale, a ferroelectric behavior corresponding to the existence of an acentric structure. Based upon this experimental evidence, the lattice parameters of the differently-sized BaTiO_3 nanocrystals have been refined with the CELREF (version 3) software using a tetragonal unit cell (non-centrosymmetric space group $P4mm$ no. 99). The values of the refined lattice parameters, the volume of the unit cell and the c/a ratio are presented in Table 2. As inferred from the values presented in Table 2, the unit cell parameters decrease with the increase in the size of the nanoparticles, whereas the c/a ratio follows an opposite trend. The increase of the unit cell volume with the decrease in the size of the nanoparticles has been commonly observed in nanoscale oxides, being ascribed to the truncation of the attractive Madelung potential responsible for the stability of the crystal structure.⁴¹ Moreover, the c/a values calculated from the refined unit cell parameters are smaller than that corresponding to the bulk material ($c/a = 1.011$)⁴² but are comparable to other values reported in the literature,⁴³ thereby confirming the existence of a tetragonal distortion in the BaTiO_3 colloidal nanocrystals synthesized by the proposed solvothermal method. Scherrer analysis of the full width at half maximum of the three most intense X-ray diffraction peaks has led to values of the crystallite size comparable to the nanoparticle size determined by electron microscopy, which suggests that the nanoparticles are single crystalline in nature, despite the relatively low temperature used in their synthesis.

The local structural distortions existing in the BaTiO_3 colloidal nanocrystals have been studied by room temperature Raman spectroscopy. It is well-known that in cubic BaTiO_3

Table 2 Refined values of the lattice parameters, unit cell volume and c/a ratio for BaTiO_3 nanopowders containing differently-sized nanoparticles

Size (nm)	8	15	22	40	78
a (Å)	4.010(2)	4.009(5)	4.006(5)	4.004(1)	4.002(9)
c (Å)	4.030(7)	4.020(1)	4.018(9)	4.016(8)	4.013(9)
V (Å ³)	64.82(1)	64.62(4)	64.51(2)	64.40(1)	64.32(6)
c/a	1.0022(9)	1.0026(4)	1.0030(9)	1.0031(7)	1.0033(2)

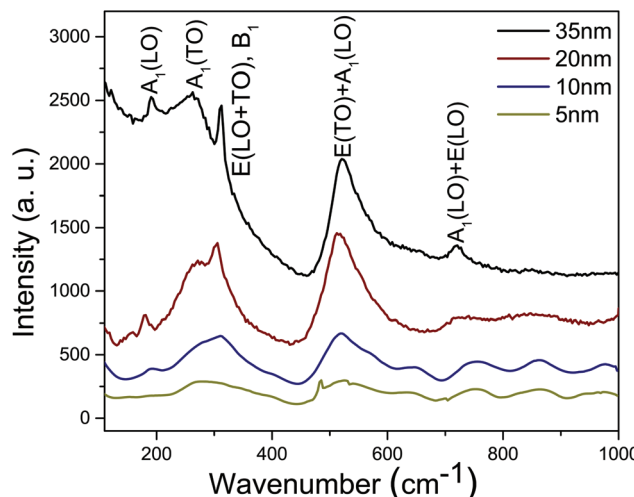


Fig. 6 Representative room-temperature Raman spectra of nanopowders containing variable-size BaTiO_3 nanocubes.

(space group $Pm3m$) the perfectly symmetrical coordination environment around the Ti^{4+} ions is associated with the $3\text{F}_{1u} + \text{F}_{2u}$ phonons, which correspond to Raman inactive modes. However, when the titanium centers undergo an off-center shift, the symmetry of the lattice will be lowered to tetragonal (space group $P4mm$), thereby giving rise to Raman active phonons represented by $3[\text{A}_1(\text{TO}) + \text{A}_1(\text{LO})] + \text{B}_1 + 4[\text{E}(\text{TO}) + \text{E}(\text{LO})]$.⁴⁴ As seen in Fig. 6, the Raman spectra of variable-sized BaTiO_3 nanocrystals feature well-defined bands located around 192, 262, 311, 529 and 720 cm^{-1} . These bands have been assigned to the $\text{E}(2(\text{TO}) + \text{E}(1\text{LO}) + \text{A}_1(\text{TO}) + \text{A}_1(\text{LO})$, $\text{A}_1(2\text{TO})$, $\text{E}(3\text{TO}) + \text{E}_2(\text{LO}) + \text{B}_1$, $\text{E}(4\text{TO}) + \text{A}_1(3\text{TO})$ and $\text{E}(4\text{LO}) + \text{A}_1(3\text{LO})$ Raman modes, thereby indicating the presence of local tetragonal distortions in the corresponding nanopowdered samples. It is worth noting that the bands at 311 and 720 cm^{-1} , which are generally considered the signature of the tetragonal structure, are well-defined and relatively strong in intensity. Furthermore, the Raman bands were found to broaden with a decrease in the size of the nanocrystals from 35 to 5 nm, which indicate that the tetragonal distortion is accompanied by a notable decrease of the structural coherence as the nanoparticle size decreases in perovskite nanocrystals.^{43a}

3.4. Solubility of the BaTiO_3 nanocrystals, surface composition and surface functionalization

The as-prepared BaTiO_3 nanocrystals are highly dispersible in non-polar solvents such as toluene or hexane as a result of the retention of oleic acid molecules on their surfaces. This will not only prevent the aggregation of the nanoparticles, but also renders them hydrophobic and dispersible in non-polar solvents with formation of very stable colloidal solutions. The existence of oleic acid molecules chemisorbed on the surface of the nanoparticles was confirmed experimentally by FT-IR spectroscopy analysis of neat oleic acid and oleic 15 nm BaTiO_3 nanocubes. The corresponding spectra indicated

strong similarities between the absorption bands appearing at 3007 cm^{-1} specific to the stretching mode of the $=\text{C}-\text{H}$ bond and those at 2934 , 2854 , 2924 and 2845 cm^{-1} , associated with the C-H (ν_{asym} and ν_{sym}) stretching modes of the long aliphatic chains (Fig. 7). The band located at 1707 cm^{-1} in the FTIR spectrum of oleic acid, corresponding to the $-\text{C}=\text{O}$ stretching mode, is shifted to higher wave numbers in the spectrum of the 15 nm BaTiO_3 nanoparticles as a result of the conversion of the carboxyl group into carboxylate COO^- ions and their subsequent coordination to the metal centers on the surface of the nanocrystals. The carboxylate ions are also associated with the bands at 1541 and 1454 cm^{-1} (ν_{asym} and ν_{sym}), whereas the bands at 1089 and 938 cm^{-1} have been assigned to the CO vibration in ether and the scissoring vibration (δ') of the CH_2 group, respectively. A key step in the design of nanoparticle-based devices, such as capacitors,⁴⁵ field effect transistors,⁴⁶ inverters,⁴⁷ integrated circuits⁴⁸ or bipolar resistive switching memory devices⁴⁹ is the design of uniform, defect-free nanocrystal-based thin films with tunable thickness on various substrates. The high quality of the perovskite cuboidal nanocrystals, as well as their ability to disperse in non-polar solvents allowed us to fabricate uniform and crack-free ferroelectric films on large surfaces by an evaporative-driven assembly process (Fig. S11 ESI†). The further annealing of these films will eliminate the intercrystal void spaces resulting from the compact assembly of the nanocrystals and densify the films, thereby making perovskite nanocubes very promising for implementation in flexible electronics. Thermal analysis experiments (not shown) indicated that the amount of oleic acid molecules retained at the surface of the BaTiO_3 cuboidal nanocrystals decreases from 9.1% to 4.1% with the increase in the particle size from 5 to 40 nm as a result of the decrease of the surface-to-volume ratio of the nanoparticles with the

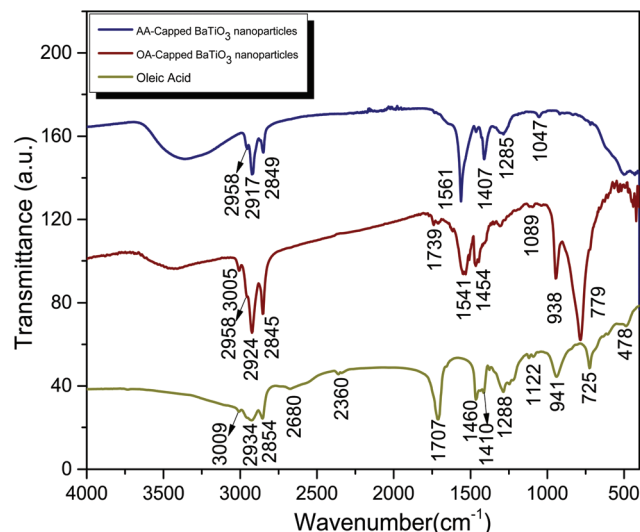


Fig. 7 FT-IR spectra of neat oleic acid (yellow curve) and 15 nm BaTiO_3 nanocrystals before (brown curve) and after (blue curve) treatment with Lemieux-von Rudloff reagent.

increase in their average edge length. It is worth noting that small nanocrystals possess an increased solubility in non-polar solvents compared with those reported previously in the literature with values of the solubility as high as 150 mg mL⁻¹ for 15 nm nanocrystals (Fig. 8b). Recently, it has been pointed out that ferroelectric perovskite nanocrystals are excellent candidates for biological and medical imaging applications by virtue of their unique non-linear optical properties such as the second harmonic generation (SHG) effect which will overcome the limitations of fluorescent dyes used as labels for conventional fluorescence microscopy.^{10a,50} A key prerequisite for the development of nanocrystal-based SHG labels is the ability of the nanoparticles to disperse in polar solvents, in particular water. We demonstrated recently that highly uniform BaTiO₃ nanocrystals obtained by the solvothermal method developed by our group are amenable to specific surface engineering. Specifically, their surface composition and polarity can be easily tuned *via* sequential ligand exchange chemistry with nitrosonium tetrafluoroborate (NOBF₄) yielding highly stable colloidal solution polar solvents, such as dimethyl formamide.⁵¹ We show herein that oleic acid-capped BaTiO₃ nanocubes can also be rendered hydrophilic and dispersible in polar solvents upon the selective oxidative cleavage of the R-C=C-R' double bond with the formation of azelaic acid which leaves free carboxyl groups anchored to the surfaces of the nanocrystals (Fig. 8a) and pelargonic acid which is eliminated upon washing.

The formation of azelaic acid molecules from oleic acid was confirmed by FTIR analysis of the resulting powders. As seen

in Fig. 7, the band at 3009 cm⁻¹, characteristic of the =C-H stretching vibration, is absent in the FTIR spectrum of the BaTiO₃ nanopowders treated with the Lemieux-von Rudloff reagent, whereas the bands at 1561 and 1407 cm⁻¹, characteristic of azelaic acid,⁵² are observed confirming that the -C=C-bond in oleic acid molecules has been oxidized to the carboxyl group. This observation was further supported by the visual inspection of a hexane solution of oleic acid-capped 15 nm BaTiO₃ before and after the oxidative cleavage (Fig. 8c). Therefore, it can be clearly seen that hydrophobic BaTiO₃ nanocubes suspended in cyclohexane are found as the top phase of a mixture containing the colloidal nanocrystals and water (left vial). After the oxidation of oleic acid the presence of azelaic acid molecules on the surface of the nanocrystals renders them hydrophilic and they are transferred across the interface from the toluene phase to the aqueous solution (right vial).

3.5. Mesoscale structures by using colloidal perovskite nanocrystals as building blocks

The precise control over the shape, size and surface composition of the perovskite nanocubes in combination with an evaporation-induced self-assembly process allowed us to use the colloidal nanocrystals as building blocks for the design of mesoscale hierarchical structures, such as 3D superlattice assemblies and superparticles. Such systems are attractive from both a fundamental and technological viewpoint, including the study of dipole–dipole interactions in ferroic or multi-ferroic systems or in the design of novel mesoscale functional materials/nanocomposites with potential applications in energy conversion and data storage. Superlattice structures of BaTiO₃ nanocubes can be easily obtained by casting a 0.1 M solution onto different substrates, such as TEM copper grids or silicon wafers followed by the slow evaporation of the solvent, whereby the nanocrystals rearrange into highly ordered, densely packed 3-D configurations.

The visual inspection of the substrates reveals the formation of nanoparticle layers with rainbow-like appearance, which is strongly indicative of the formation of long range ordered arrays of nanocrystals.⁵³ To gain insight into the type of long-range arrangement formed by these nanocubes *via* self-assembly we examined carefully the TEM micrographs of BaTiO₃ nanocrystals dispersed in different non-polar solvents, such as toluene and hexane, respectively. As seen in Fig. 9, when toluene solutions containing oleic acid-capped monodisperse 10 nm BaTiO₃ nanocubes are cast on solid substrates, the nanocubes self-assemble with formation of monolayers and superlattice structures. The resulting nanoparticle superlattices are constructed by the ordered packing of individual 10 nm BaTiO₃ nanocubes. Moreover, the nanocubes are crystallographically aligned, being connected with the adjacent counterparts *via* the (001) facets. Such an observation is strongly supported by the X-ray diffraction pattern of the nanoparticle superlattices, which show intense peaks corresponding to the (100), (200) and (300) reflections compared to those observed in the pattern of the bulk material. Specifically, while their relative intensities were 14, 35 and 5% in bulk

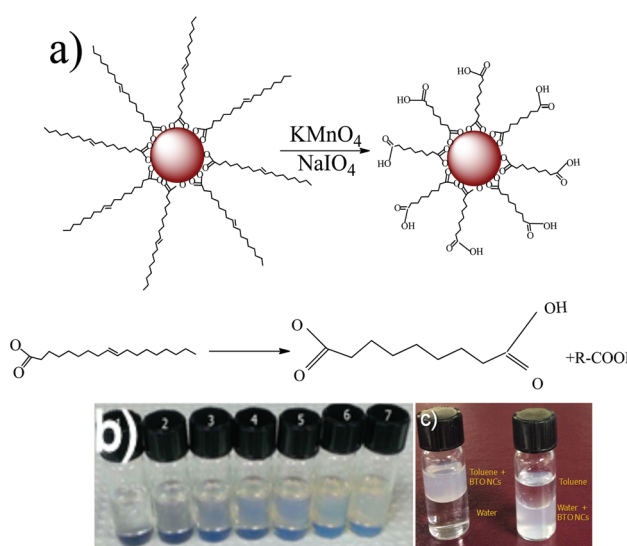


Fig. 8 (a) Scheme depicting the conversion of oleic acid into azelaic acid onto the surface of the nanocrystals upon their treatment with Lemieux–von Rudloff reagent. (b) Pictures of toluene solutions of 15 nm BaTiO₃ nanocubes in which the concentration of the nanoparticles varied from 9.75 (vial no. 1) to 18.75, 37.5, 56.5, 75, 112.5 and 150 mg mL⁻¹ (vial no. 2–7, respectively). (c) Picture of cyclohexane and water mixtures containing 15 nm BaTiO₃ nanocubes before (left vial) and after (right vial) treatment with the Lemieux–von Ruddoff reagent.

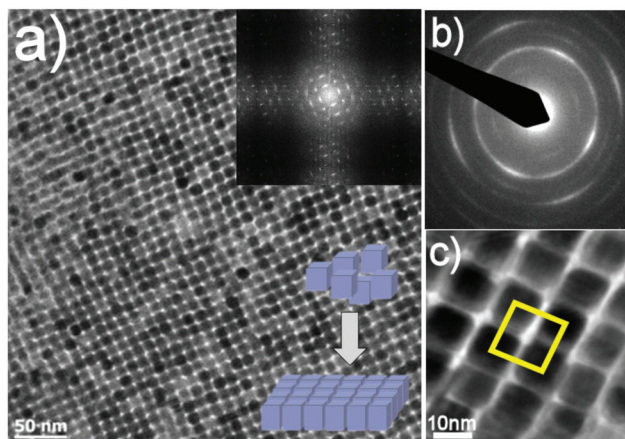


Fig. 9 Low magnification (a) and high magnification (c) TEM images of simple cubic (sc) superlattice structures formed by monodisperse 10 nm BaTiO₃ nanocubes. (b) Selected area electron diffraction (SAED) pattern of the superlattice assembly. The top right inset in (a) shows the fast Fourier transform (FFT) pattern of the TEM image.

BaTiO₃ (PDF no. 31–174) the observed relative intensities of the (100), (200) and (300) reflections in the self-assemblies were 68, 127.8 and 26%, respectively (Fig. SI2†). These results are similar to those observed by Chen and coworkers in the case of the oriented self-assembly of Fe₅₀Pt₅₀ nanocubes.⁵⁴ Moreover, such an arrangement has been commonly observed in the case of other oxides, such as In₂O₃,⁵⁵ Fe_xO_y,⁵⁶ spinel ferrites CoFe₂O₄⁵⁷ or metals, such as Pt⁵⁸ and corresponds to a simple cubic (sc) mesostructure (space group Pm3m no. 221).

The uniformity in shape and size is a key parameter in successfully designing highly regular 3-D arrays and our experimental results further confirm the reliability of the proposed approach with respect to the synthesis of high quality perovskite nanoparticles. The superlattice structures are extended over several square inches (Fig. 9a) and consist of a few nanoparticle monolayers. The superlattice parameter can be calculated from the spacing between the centers of two adjacent cubes and the value obtained experimentally in the case of BaTiO₃ nanocube-based 3-D ordered arrays is 12.4 nm (Fig. 9c). A close inspection of the selected area electron diffraction (SAED) patterns of a monolayer of nanoparticles and a 3-D superlattice structure (Fig. 9b) reveals that the diffraction rings observed for the monolayer are elongated with the most intense diffraction spots attributed to the (200) planes, thereby indicating that the majority of nanocubes in the superlattice structure possess a similar spatial orientation as a result of the alignment of their axes along this crystallographic direction during the self-assembly process. Cao *et al.* suggested that unlike spheroidal nanocrystals, which conventionally assemble into compact hexagonal arrangements, cuboidal nanoparticles form superlattice structures with a simple cubic symmetry to minimize their bulk free energy ($G = NE_p$; where G stands for the bulk free energy, N is the total number of closest nanocube contacts and E_p is the energy of interaction between two adjacent

nanocubes, respectively).¹⁵ However, Quan and coworkers pointed out that the type of solvent plays an important role in the type of symmetry adopted by 3-D regular arrays formed from non-spheroidal monodisperse nanoparticles since such morphologies make possible the fine tuning of the ligand–ligand–solvent interactions and stabilize a body-centered tetragonal structure in addition to the simple cubic symmetry of the superlattice.⁵³ Interestingly, when hexane solutions of monodisperse 10 nm BaTiO₃ nanocubes were cast on planar substrates followed by the slow evaporation of the solvent the nanocubes constructing the superlattice share their corners instead of their faces as in the case of hierarchical assemblies obtained from BaTiO₃ dispersed in toluene (Fig. 10). The inset of Fig. 10a represents the fast Fourier transform (FFT) of the nanoparticle assembly along the [001] direction showing that the superlattice structure presents a four-fold symmetry. Chan and coworkers reported the formation of superlattices with different packing behaviors of the constituting nanoparticles obtained by self-assembly of colloidal octylamine-coated 5 nm cuboidal nanocrystals dispersed in toluene.⁵⁹

According to them, regular cubes self-assemble into simple cubic superlattices in which the constituting nanoparticles are stacked on top of each other and share the (001) faces, whereas cuboidal nanoparticles with slightly truncated corners yield supercrystals with a packing fcc structure instead of a simple cubic structure. The origin of such a change in the packing symmetry of the nanocubes has been tentatively ascribed to the existence of a charge transfer between the metallic nanoparticles and the capping ligand molecules which induces a Coulomb coupling between electrostatic fields associated with the charged nanoparticles. However, in the case of BaTiO₃ superlattice structures obtained from hexane, the similarity of the selected area electron diffraction (SAED) patterns (Fig. 9b and 10b), which present four intense,

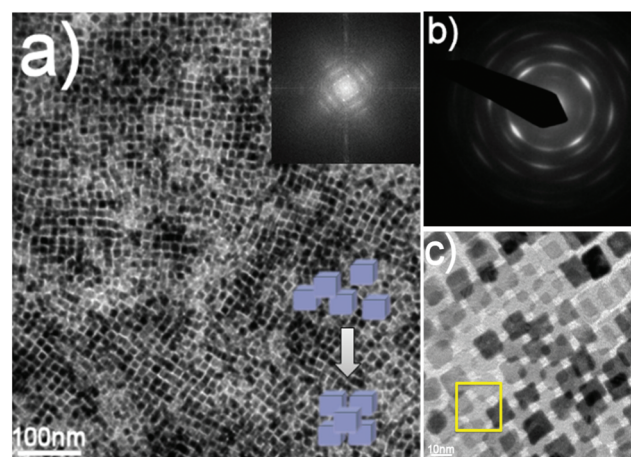


Fig. 10 Low magnification (a) and high magnification (c) TEM images of bct superlattice structures formed by monodisperse 10 nm BaTiO₃ nanocubes. (b) Selected area electron diffraction (SAED) pattern of the superlattice assembly. The top right inset in a shows the fast Fourier transform (FFT) pattern of the TEM image.

elongated diffraction spots associated with the (200) planes, suggests that these assemblies adopt a body centered tetragonal (bct) packing structure (space group $I4/mmm$ no. 139) instead of an fcc structure. The BaTiO_3 superlattice assemblies are similar to those observed by Quan *et al.* in the case of Pt nanocube superlattices by using electron tomography. Specifically, these structures are constructed by alternate layers in which monodisperse nanocubes share their faces and are separated by layers in which the nanocubes are shifted by a certain distance along the diagonal between two adjacent nanocubes (see the scheme in Fig. 10a). A detailed investigation of the packing symmetries of BaTiO_3 cuboidal nanostructures into different types of superlattices, as well as the factors influencing these types of assemblies is currently underway and will be reported in a forthcoming paper.

Other types of hierarchical assemblies can be also derived by uniformly packing monodisperse BaTiO_3 nanocubes obtained by this colloidal chemistry technique. For example, when 0.1 M solutions of nanocrystals were cast on substrates followed by the slow evaporation of the solvent, 3-D hierarchical structures such as perovskite superparticles can be obtained (Fig. 11). Although many types of superparticles of uniformly-sized nanocrystals, including magnetic and semiconductor colloidal nanoparticles, (Fe_3O_4 ,¹⁵ PbSe ,⁶⁰ Au and CdSe-CdS ⁶¹) have been previously synthesized, to our knowledge this is the first experimental evidence about the design of superparticles constructed from individual monodisperse ferroelectric nanocrystals. The morphology of the BaTiO_3 superparticles was investigated by electron microscopy and atomic force microscopy. From the image contrast in Fig. 11a it can be clearly seen that the light background corresponds to a monolayer formed by 8 nm monodisperse nanocubes, whereas the darker areas indicate the formation of superparti-

cles with an average edge length which extends up to 500 nm. Superparticles appear to be free of defects and present a high degree of both orientational and translational order (Fig. SI3†) similar to those observed in the case of the BaTiO_3 superlattice structures. The true 3-D nature of these assemblies has been demonstrated by field-emission scanning electron microscopy (FE-SEM) (Fig. 11b) and atomic force microscopy experiments (Fig. 11c), which reveal the presence of distinct superparticles lying on the substrate. These superparticles present well-defined faces and an average edge length of 500 nm. Due to their unique morphological characteristics and since such hierarchical structures are expected to harness both the properties of the individual constituting nanocrystals and those originating from the interaction and mutual influence of the nanoparticles, they are potentially interesting systems for both fundamental studies of ferroelectricity at the nanoscale and technological applications in data storage, catalysis and energy conversion/storage.

3.6. Preparation of other perovskite colloidal nanocrystals

To demonstrate the generality of the proposed synthetic approach perovskite nanocrystals with other chemical compositions have been prepared using an experimental protocol similar to that used for the synthesis of 10 nm BaTiO_3 nanocubes. Fig. 12 shows representative electron microscopy images of BaZrO_3 (Fig. 12a–c), PbTiO_3 (Fig. 12d and e) and SrTiO_3 colloidal nanocrystals obtained by the solvothermal treatment of the reaction precursors at 180 °C for 48 h (Fig. 12f). The TEM images show that regardless of their chemical composition perovskite nanoparticles are well-separated with a narrow size distribution and retain oleic acid molecules on their surfaces. Interestingly, their shape was found to vary from cubic for BaZrO_3 , and PbTiO_3 to spheroidal for

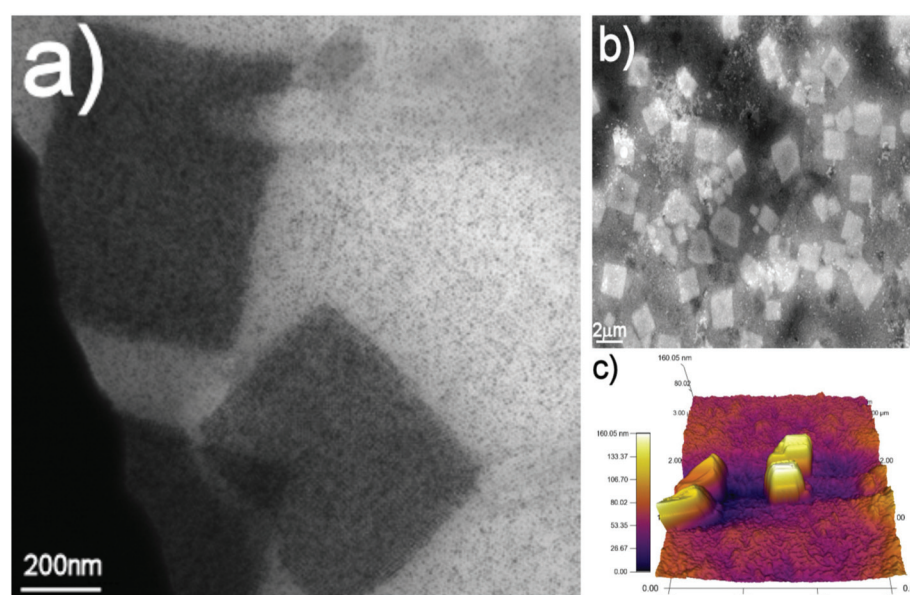


Fig. 11 TEM (a), FE-SEM (b) and AFM height images (c) of superparticle structures formed by 8 nm BaTiO_3 monodisperse nanocubes.

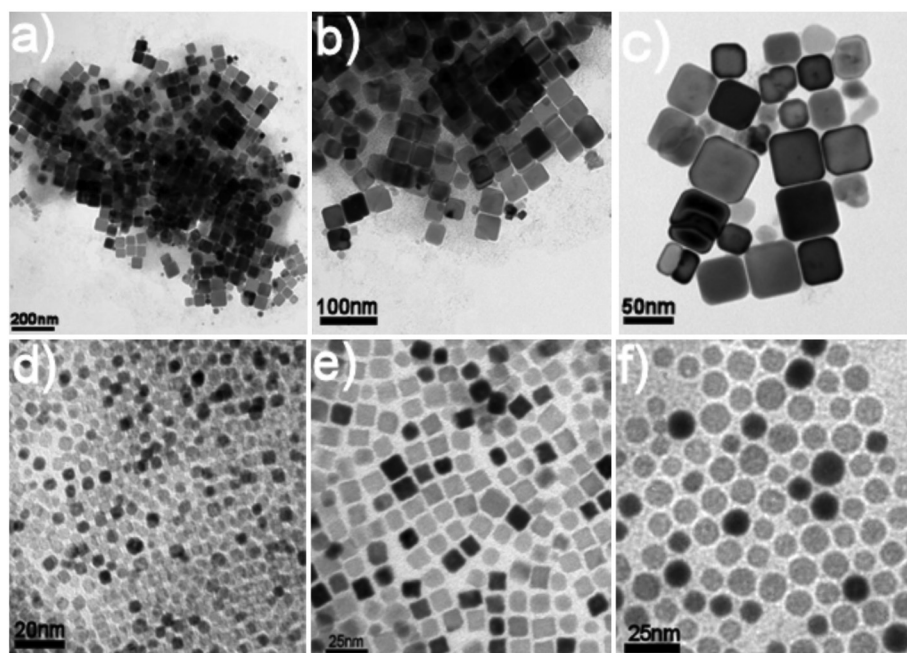


Fig. 12 TEM images of 50 nm BaZrO_3 (a–c), 4 nm and 20 nm PbTiO_3 (d, e) PbTiO_3 nanocubes and (f) 12 nm SrTiO_3 spheroidal nanoparticles.

SrTiO_3 nanocrystals. Preliminary experiments have also shown that the size of the perovskite nanocrystals can be controlled by varying the concentration of the reaction precursors. For example, the size of the PbTiO_3 nanocrystals increased from 4 to 20 nm when the concentration of PbNO_3 and Ti(OBu)_4 in the reaction solution was changed from 2 mM to 0.5 mM. Syntheses of perovskite colloidal nanocrystals with various chemical compositions and sizes/shapes, as well as a systematic study on the influence of various reaction conditions on their size and shape are currently underway and will be reported in a forthcoming paper.

4. Conclusions

In summary, highly uniform perovskite colloidal nanocrystals have been prepared by a highly versatile solvothermal route at temperatures below 200 °C. Perovskite nanocrystals with various sizes and shapes can be obtained by changing various reaction parameters, such as the concentration of the precursors in solution, the polarity of the solvent and the reaction time. The as-prepared nanoparticles are hydrophobic being passivated with oleic acid molecules on their surfaces, which enable them to form highly stable colloidal solutions in non-polar solvents. However, upon the oxidative cleavage of the oleic acid treatment with the Lemieux-von Ruddloff reagent, the surfactant molecules are converted into azelaic acid, thereby rendering the perovskite nanocrystals hydrophilic and dispersible in polar solvents, such as alcohols or water. Regardless of their size, the BaTiO_3 nanocrystals present an acentric structure associated with the off-center shift of the

Ti^{4+} ions within the unit cell, with a c/a value which increases from 1.0022(9) to 1.0033(2) when the size of the nanocrystals was varied from 8 to 78 nm. As a result of their uniformity in size and shape, quasi-monodisperse perovskite nanocrystals can be organized into superlattices and superparticles. The superlattice structure was found to depend on the type of solvent used, that is while toluene solutions of perovskite nanoparticles yield simple cubic (sc) mesostructures (space group $Pm\bar{3}m$ no. 221), nanocrystals dispersed in hexane form superlattice assemblies with a body centered tetragonal (bct) structure (space group $I4/mmm$ no. 139). Perovskite nanocubes with well-defined sizes and shapes synthesized by this approach can be used as a model system for the study of the ferroelectric order at the nanoscale or as building blocks for the design of various types of functional materials, such as highly magnetoelectric nanocomposite superlattice structures, which may exhibit novel magnetic, electric and magnetoelectric properties.

Competing interest

The authors declare no competing financial interest.

Acknowledgements

This work was supported by the National Science Foundation (NSF) through the CAREER grant no. 1434457 and the Central Michigan University through start-up funds.

References

- 1 Z. Yan, Y. Guo, G. Zhang and J. M. Liu, High-Performance Programmable Memory Devices Based on Co-Doped BaTiO₃, *Adv. Mater.*, 2011, **23**(11), 1351–1355.
- 2 (a) Y. Inoue, K. Sato, K. Sato and H. Miyama, Photoassisted water decomposition by ferroelectric lead zirconate titanate ceramics with anomalous photovoltaic effects, *J. Phys. Chem.*, 1986, **90**(13), 2809–2810; (b) K. Maeda, Rhodium-Doped Barium Titanate Perovskite as a Stable p-Type Semiconductor Photocatalyst for Hydrogen Evolution under Visible Light, *ACS Appl. Mater. Interfaces*, 2014, **6**(3), 2167–2173; (c) K. S. Hong, H. F. Xu, H. Konishi and X. C. Li, Direct Water Splitting Through Vibrating Piezoelectric Microfibers in Water, *J. Phys. Chem. Lett.*, 2010, **1**(6), 997–1002.
- 3 J. Li, J. Claude, L. E. Norena-Franco, S. I. Seok and Q. Wang, Electrical Energy Storage in Ferroelectric Polymer Nanocomposites Containing Surface-Functionalized BaTiO₃ Nanoparticles, *Chem. Mater.*, 2008, **20**(20), 6304–6306.
- 4 (a) S. Tao and J. T. S. Irvine, A redox-stable efficient anode for solid-oxide fuel cells, *Nat. Mater.*, 2003, **2**(5), 320–323; (b) S. Siahrostami, M. E. Bjorketun, P. Strasser, J. Greeley and J. Rossmeisl, Tandem cathode for proton exchange membrane fuel cells, *Phys. Chem. Chem. Phys.*, 2013, **15**(23), 9326–9334.
- 5 (a) L. Bocher, A. Gloter, A. Crassous, V. Garcia, K. March, A. Zobelli, S. Valencia, S. Enouz-Vedrenne, X. Moya, N. D. Marthur, C. Deranlot, S. Fusil, K. Bouzehouane, M. Bibes, A. Barthélémy, C. Colliex and O. Stéphan, Atomic and Electronic Structure of the BaTiO₃/Fe Interface in Multiferroic Tunnel Junctions, *Nano Lett.*, 2011, **12**(1), 376–382; (b) J. Y. Son, J.-H. Lee, S. Song, Y.-H. Shin and H. M. Jang, Four-States Multiferroic Memory Embodied Using Mn-Doped BaTiO₃ Nanorods, *ACS Nano*, 2013, **7**(6), 5522–5529.
- 6 (a) R. O. Cherifi, V. Ivanovskaya, L. C. Phillips, A. Zobelli, I. C. Infante, E. Jacquet, V. Garcia, S. Fusil, P. R. Briddon, N. Guiblin, A. Mougin, A. A. Ünal, F. Kronast, S. Valencia, B. Dkhil, A. Barthélémy and M. Bibes, Electric-field control of magnetic order above room temperature, *Nat. Mater.*, 2014, **13**(4), 345–351; (b) M. Bibes, N. Reyren, E. Lesne, J.-M. George, C. Deranlot, S. Collin, A. Barthélémy and H. Jaffrès, Towards electrical spin injection into LaAlO₃–SrTiO₃, *Philos. Trans. R. Soc., A*, 2012, **370**(1977), 4958–4971.
- 7 I. Grinberg, D. V. West, M. Torres, G. Gou, D. M. Stein, L. Wu, G. Chen, E. M. Gallo, A. R. Akbashev, P. K. Davies, J. E. Spanier and A. M. Rappe, Perovskite oxides for visible-light-absorbing ferroelectric and photovoltaic materials, *Nature*, 2013, **503**(7477), 509–512.
- 8 R. M. Corn and D. A. Higgins, Optical second harmonic generation as a probe of surface chemistry, *Chem. Rev.*, 1994, **94**(1), 107–125.
- 9 E. Brown, T. McKee, E. diTomaso, A. Pluen, B. Seed, Y. Boucher and R. K. Jain, Dynamic imaging of collagen and its modulation in tumors *in vivo* using second-harmonic generation, *Nat. Med.*, 2003, **9**(6), 796–800.
- 10 (a) E. Kim, A. Steinbrück, M. T. Buscaglia, V. Buscaglia, T. Pertsch and R. Grange, Second-Harmonic Generation of Single BaTiO₃ Nanoparticles down to 22 nm Diameter, *ACS Nano*, 2013, **7**(6), 5343–5349; (b) J. Čulić-Viskota, W. P. Dempsey, S. E. Fraser and P. Pantazis, Surface functionalization of barium titanate SHG nanoprobes for *in vivo* imaging in zebrafish, *Nat. Protoc.*, 2012, **7**(9), 1618–1633.
- 11 (a) M. H. Frey and D. A. Payne, Grain-size effect on structure and phase transformations for barium titanate, *Phys. Rev. B: Condens. Matter*, 1996, **54**(5), 3158–3168; (b) T. M. Shaw, S. Trolier-McKinstry and P. C. McIntyre, THE PROPERTIES OF FERROELECTRIC FILMS AT SMALL DIMENSIONS, *Annu. Rev. Mater. Sci.*, 2000, **30**(1), 263–298.
- 12 (a) J. E. Spanier, A. M. Kolpak, J. J. Urban, I. Grinberg, L. Ouyang, W. S. Yun, A. M. Rappe and H. Park, *Nano Lett.*, 2006, **6**, 735; (b) L. Cao, B. Garipcan, E. M. Gallo, S. S. Nonnenmann, B. Nabet and J. E. Spanier, Excitation of local field enhancement on silicon nanowires, *Nano Lett.*, 2008, **8**(2), 601–605.
- 13 W. Cheng, M. J. Campolongo, S. J. Tan and D. Luo, Free-standing ultrathin nano-membranes *via* self-assembly, *Nano Today*, 2009, **4**(6), 482–493.
- 14 C. B. Murray, C. R. Kagan and M. G. Bawendi, Synthesis and characterization of monodisperse nanocrystals and close-packed nanocrystal assemblies, *Annu. Rev. Mater. Sci.*, 2000, **30**, 545–610.
- 15 T. Wang, X. Wang, D. LaMontagne, Z. Wang, Z. Wang and Y. C. Cao, Shape-Controlled Synthesis of Colloidal Superparticles from Nanocubes, *J. Am. Chem. Soc.*, 2012, **134**(44), 18225–18228.
- 16 M. P. Pilani, 2D superlattices and 3D supracrystals of metal nanocrystals: a new scientific adventure, *J. Mater. Chem.*, 2011, **21**(42), 16748–16758.
- 17 D. V. Talapin, E. V. Shevchenko, C. B. Murray, A. V. Titov and P. Král, Dipole–Dipole Interactions in Nanoparticle Superlattices, *Nano Lett.*, 2007, **7**(5), 1213–1219.
- 18 A. Dong, J. Chen, P. M. Vora, J. M. Kikkawa and C. B. Murray, Binary nanocrystal superlattice membranes self-assembled at the liquid-air interface, *Nature*, 2010, **466**(7305), 474–477.
- 19 (a) T. Ould-Ely, M. Luger, L. Kaplan-Reinig, K. Niesz, M. Doherty and D. E. Morse, Large-scale engineered synthesis of BaTiO₃ nanoparticles using low-temperature bioinspired principles, *Nat. Protoc.*, 2011, **6**(1), 97–104; (b) N. Nuraje, K. Su, A. Haboosheh, J. Samson, E. P. Manning, N.l. Yang and H. Matsui, Room Temperature Synthesis of Ferroelectric Barium Titanate Nanoparticles Using Peptide Nanorings as Templates, *Adv. Mater.*, 2006, **18**(6), 807–811.
- 20 (a) Y. Hakuta, H. Ura, H. Hayashi and K. Arai, Continuous Production of BaTiO₃ Nanoparticles by Hydrothermal Synthesis, *Ind. Eng. Chem. Res.*, 2005, **44**(4), 840–846; (b) F. A. Rabuffetti and R. L. Brutchey, Tailoring the Mecha-

- nism of the Amorphous-to-Crystalline Phase Transition of PbTiO_3 via Kinetically Controlled Hydrolysis, *Chem. Mater.*, 2011, **23**(17), 4063–4076.
- 21 L. Huang, Z. Chen, J. D. Wilson, S. Banerjee, R. D. Robinson, I. P. Herman, R. Laibowitz and S. O'Brien, Barium titanate nanocrystals and nanocrystal thin films: Synthesis, ferroelectricity, and dielectric properties, *J. Appl. Phys.*, 2006, **100**(3), 415602.
- 22 H. Du, S. Wohlrab, M. Weiss and S. Kaskel, Preparation of BaTiO_3 nanocrystals using a two-phase solvothermal method, *J. Mater. Chem.*, 2007, **17**(43), 4605–4610.
- 23 F. Dang, K. Mimura, K. Kato, H. Imai, S. Wada, H. Haneda and M. Kuwabara, In situ growth BaTiO_3 nanocubes and their superlattice from an aqueous process, *Nanoscale*, 2012, **4**(4), 1344–1349.
- 24 M. Niederberger, N. Pinna, J. Polleux and M. Antonietti, A General Soft-Chemistry Route to Perovskites and Related Materials: Synthesis of BaTiO_3 , BaZrO_3 , and LiNbO_3 Nanoparticles, *Angew. Chem., Int. Ed.*, 2004, **43**(17), 2270–2273.
- 25 S. Adireddy, C. Lin, B. Cao, W. Zhou and G. Caruntu, Solution-Based Growth of Monodisperse Cube-Like BaTiO_3 Colloidal Nanocrystals, *Chem. Mater.*, 2010, **22**(6), 1946–1948.
- 26 M. J. Polking, M. G. Han, A. Yourdkhani, V. Petkov, C. F. Kisielowski, V. V. Volkov, Y. M. Zhu, G. Caruntu, A. P. Alivisatos and R. Ramesh, Ferroelectric order in individual nanometre-scale crystals, *Nat. Mater.*, 2012, **11**(8), 700–709.
- 27 Z. Chen, H. Chen, H. Hu, M. Yu, F. Li, Q. Zhang, Z. Zhou, T. Yi and C. Huang, Versatile Synthesis Strategy for Carboxylic Acid-functionalized Upconverting Nanophosphors as Biological Labels, *J. Am. Chem. Soc.*, 2008, **130**(10), 3023–3029.
- 28 (a) S. Wolfgang, P. Georgios and D. Amit, *Theory and Applications of Colloidal Processing*, in *Chemical Processing of Ceramics*, CRC Press, 2nd edn, 2005, pp. 269–302; (b) C. J. Brinker and G. W. Scherer, *Sol-Gel Science: The Physics and Chemistry of Sol-Gel Processing*, 1990; (c) Y. Murakami, T. Matsumoto and Y. Takasu, Salt Catalysts Containing Basic Anions and Acidic Cations for the Sol-Gel Process of Titanium Alkoxide: Controlling the Kinetics and Dimensionality of the Resultant Titanium Oxide, *J. Phys. Chem. B*, 1999, **103**(11), 1836–1840.
- 29 H. Fric and U. Schubert, Amine adducts of titanium tetraalkoxides, *New J. Chem.*, 2005, **29**(1), 232–236.
- 30 (a) H. Fric, M. Puchberger and U. Schubert, Contributions to the Structural Chemistry of 2-Amino Alcoholate Derivatives of Titanium and Zirconium Alkoxides and Their Partial Hydrolysis Products, *Eur. J. Inorg. Chem.*, 2008, **2008**(9), 1452–1461; (b) U. Schubert, Chemical modification of titanium alkoxides for sol-gel processing, *J. Mater. Chem.*, 2005, **15**(35–36), 3701–3715.
- 31 A. Singh, C. K. Sharma, A. K. Rai, V. D. Gupta and R. C. Mehrotra, Reactions of oximes and diethylhydroxylamine with titanium alkoxides, *J. Chem. Soc. A*, 1971, (0), 2440–2444.
- 32 P. D. Moran, C. E. F. Rickard, G. A. Bowmaker, R. P. Cooney, J. R. Bartlett and J. L. Woolfrey, X-ray Structure and Raman Spectrum of $[\text{Ti}4(\mu_3\text{-O})2(\mu_2\text{-O}i\text{Pr})2(\text{O}i\text{Pr})8\text{-acac}2]$: Presence of a $\text{Ti}4(\mu_3\text{-O})2(\mu_2\text{-O}i\text{Pr})2$ Ladder-like Core, *Inorg. Chem.*, 1998, **37**(6), 1417–1419.
- 33 N. Miele-Pajot, G. Hubert-Pfalzgraf, R. Papiernik, J. Vaissermann and R. Collier, Synthesis and molecular structure of $[\text{Ti}4(\text{OPri})8\text{[small micro][small eta]2-OCH}_2\text{CH[double bond, length as m-dash]CHCH}_2\text{O}2\text{[small micro]3,[small eta]2-OCH}_2\text{CH[double bond, length as m-dash]CHCH}_2\text{O}2]$. Application to the elaboration of low density, microcellular, doped organic materials, *J. Mater. Chem.*, 1999, **9**(12), 3027–3033.
- 34 (a) U. Schubert, E. Arpac, W. Glaubitt, A. Helmerich and C. Chau, Primary hydrolysis products of methacrylate-modified titanium and zirconium alkoxides, *Chem. Mater.*, 1992, **4**(2), 291–295; (b) P. D. Cozzoli, A. Kornowski and H. Weller, Low-Temperature Synthesis of Soluble and Processable Organic-Capped Anatase TiO_2 Nanorods, *J. Am. Chem. Soc.*, 2003, **125**(47), 14539–14548; (c) R. N. Kapoor and R. C. Mehrotra, 76. Organic compounds of zirconium. Part VI. Reactions of zirconium tetrachloride and isopropoxide with fatty acids, *J. Chem. Soc.*, 1959, (0), 422–426; (d) P. H. Mutin, G. Guerrero and A. Vioux, Hybrid materials from organophosphorus coupling molecules, *J. Mater. Chem.*, 2005, **15**(35–36), 3761–3768.
- 35 S. K. Lee, T. J. Park, G. J. Choi, K. K. Koo and S. W. Kim, Effects of KOH/BaTi and Ba/Ti ratios on synthesis of BaTiO_3 powder by coprecipitation/hydrothermal reaction, *Mater. Chem. Phys.*, 2003, **82**(3), 742–749.
- 36 L. Hu, C. Wang, S. Lee, R. E. Winans, L. D. Marks and K. R. Popeppelmeyer, SrTiO_3 Nanocuboids form a Lamellar Microemulsion, *Chem. Mater.*, 2013, **25**(3), 378.
- 37 C. Friderichs, N. Zotov and W. Mader, Synthesis of Monodisperse $\text{SrTi}_{1-x}\text{Zr}_x\text{O}_3$ Nanocubes in Oleate by a Two-Phase Solvothermal Method, *Eur. J. Inorg. Chem.*, 2015, **2**, 288.
- 38 L. Wu, P.-O. Jubert, D. Berman, W. Imai, A. Nelson, H. Zhu, S. Zhang and S. Sun, Monolayer Assembly of Ferromagnetic $\text{CoxFe}_{3-x}\text{O}_4$ Nanocubes for Magnetic Recording, *Nano Lett.*, 2014, **14**(6), 3395–3399.
- 39 (a) A. Testinon, M. T. Buscaglia, M. Viviani, V. Buscaglia and P. Nanni, Synthesis of BaTiO_3 Particles with Tailored Size by Precipitation from Aqueous Solutions, *J. Am. Ceram. Soc.*, 2004, **87**(1), 79–83; (b) Q. Ma, K. Kato and K.-i. Mimura, Diversity in Size of Barium Titanate Nanocube Synthesized by Hydrothermal Method Using Aqueous Ti Compound, *CrystEngComm*, 2014, **16**, 8398; (c) A. Habib, R. Haubner and N. Stelzer, Effect of temperature, time and particle size of Ti precursor on hydrothermal synthesis of barium titanate, *Mater. Sci. Eng. B*, 2008, **152**(1–3), 60–65.
- 40 V. K. LaMer and R. H. Dinegar, Theory, Production and Mechanism of Formation of Monodispersed Hydrosols, *J. Am. Chem. Soc.*, 1950, **72**(11), 4847–4854.
- 41 V. Perebeinos, S.-W. Chan and F. Zhang, ‘Madelung model’ prediction for dependence of lattice parameter on

- nano crystal size, *Solid State Commun.*, 2002, **123**(6–7), 295–297.
- 42 G. H. Kwei, A. C. Lawson, S. J. L. Billinge and S. W. Cheong, Structures of the ferroelectric phases of barium titanate, *J. Phys. Chem.*, 1993, **97**(10), 2368–2377.
- 43 (a) M. B. Smith, K. Page, T. Siegrist, P. L. Redmond, E. C. Walter, R. Seshadri, L. E. Brus and M. L. Steigerwald, Crystal Structure and the Paraelectric-to-Ferroelectric Phase Transition of Nanoscale BaTiO₃, *J. Am. Chem. Soc.*, 2008, **130**(22), 6955–6963; (b) M. L. Moreira, G. P. Mambrini, D. P. Volanti, E. R. Leite, M. O. Orlando, P. S. Pizani, V. R. Mastelaro, C. O. Paiva-Santos, E. Longo and J. A. Varela, Hydrothermal Microwave: A New Route to Obtain Photoluminescent Crystalline BaTiO₃ Nanoparticles, *Chem. Mater.*, 2008, **20**(16), 5381–5387; (c) H.-W. Lee, S. Moon, C.-H. Choi and D. K. Kim, Synthesis and Size Control of Tetragonal Barium Titanate Nanopowders by Facile Solvothermal Method, *J. Am. Ceram. Soc.*, 2012, **95**(8), 2429–2434.
- 44 U. D. Venkateswaran, V. M. Naik and R. Naik, High-pressure Raman studies of polycrystalline BaTiO₃, *Phys. Rev. B: Condens. Matter*, 1998, **58**(21), 14256–14260.
- 45 L. Huang, Z. Jia, I. Kymmissis and S. O'Brien, High K Capacitors and OFET Gate Dielectrics from Self-Assembled BaTiO₃ and (Ba,Sr)TiO₃ Nanocrystals in the Superparaelectric Limit, *Adv. Funct. Mater.*, 2010, **20**(4), 554–560.
- 46 S. J. Oh, Z. Wang, N. E. Berry, J.-H. Choi, T. Zhao, E. A. Gaulding, T. Paik, Y. Lai, C. B. Murray and C. R. Kagan, Engineering Charge Injection and Charge Transport for High Performance PbSe Nanocrystal Thin Film Devices and Circuits, *Nano Lett.*, 2014, 6210.
- 47 W.-k. Koh, S. R. Saudari, A. T. Fafarman, C. R. Kagan and C. B. Murray, Thiocyanate-Capped PbS Nanocubes: Ambipolar Transport Enables Quantum Dot Based Circuits on a Flexible Substrate, *Nano Lett.*, 2011, **11**(11), 4764–4767.
- 48 D. K. Kim, Y. Lai, B. T. Diroll, C. B. Murray and C. R. Kagan, Flexible and low-voltage integrated circuits constructed from high-performance nanocrystal transistors, *Nat. Commun.*, 2012, **3**, 1216.
- 49 Y. Kim, K. Kook, S. K. Hwang, C. Park and J. Cho, Polymer/Perovskite-Type Nanoparticle Multilayers with Multielectric Properties Prepared from Ligand Addition-Induced Layer-by-Layer Assembly, *ACS Nano*, 2014, **8**(3), 2419–2430.
- 50 P. Pantazis, J. Maloney, D. Wu and S. E. Fraser, Second harmonic generating (SHG) nanoprobes for in vivo imaging, *Proc. Natl. Acad. Sci. U. S. A.*, 2010, **107**(33), 14535–14540.
- 51 S. Salemizadeh Parizi, A. Mellinger and G. Caruntu, Ferroelectric Barium Titanate Nanocubes as Capacitive Building Blocks for Energy Storage Applications, *ACS Appl. Mater. Interfaces*, 2014, **6**, 17506.
- 52 A. Nattkemper, T. Schleiden, J. M. Migliavacca and T. Melin, Monitoring Crystallization Kinetics of Azelaic Acid by *in situ* FTIR Spectroscopy in Three-Phase Systems, *Chem. Eng. Technol.*, 2003, **26**(8), 881–889.
- 53 Z. Quan, H. Xu, C. Wang, X. Wen, Y. Wang, J. Zhu, R. Li, C. J. Sheehan, Z. Wang, D.-M. Smilgies, Z. Luo and J. Fang, Solvent-Mediated Self-Assembly of Nanocube Superlattices, *J. Am. Chem. Soc.*, 2014, **136**(4), 1352–1359.
- 54 M. Chen, J. Kim, J. P. Liu, H. Fan and S. Sun, Synthesis of FePt Nanocubes and Their Oriented Self-Assembly, *J. Am. Chem. Soc.*, 2006, **128**(22), 7132–7133.
- 55 C. H. Lee, M. Kim, T. Kim, A. Kim, J. Paek, J. W. Lee, S.-Y. Choi, K. Kim, J.-B. Park and K. Lee, Ambient Pressure Syntheses of Size-Controlled Corundum-type In₂O₃ Nanocubes, *J. Am. Chem. Soc.*, 2006, **128**(29), 9326–9327.
- 56 F. X. Redl, C. T. Black, G. C. Papaefthymiou, R. L. Sandstrom, M. Yin, H. Zeng, C. B. Murray and S. P. O'Brien, Magnetic/Electronic, and Structural Characterization of Nonstoichiometric Iron Oxides at the Nanoscale, *J. Am. Chem. Soc.*, 2004, **126**(44), 14583–14599.
- 57 Q. Song and Z. J. Zhang, Shape Control and Associated Magnetic Properties of Spinel Cobalt Ferrite Nanocrystals, *J. Am. Chem. Soc.*, 2004, **126**(19), 6164–6168.
- 58 J. Ren and R. D. Tilley, Preparation, Self-Assembly, and Mechanistic Study of Highly Monodispersed Nanocubes, *J. Am. Chem. Soc.*, 2007, **129**(11), 3287–3291.
- 59 H. Chan, A. Demortière, L. Vukovic, P. Král and C. Petit, Colloidal Nanocube Supercrystals Stabilized by Multipolar Coulombic Coupling, *ACS Nano*, 2012, **6**(5), 4203–4213.
- 60 Y. Nagaoka, O. Chen, Z. Wang and Y. C. Cao, Structural Control of Nanocrystal Superlattices Using Organic Guest Molecules, *J. Am. Chem. Soc.*, 2012, **134**(6), 2868–2871.
- 61 (a) T. Wang, J. Zhuang, J. Lynch, O. Chen, Z. Wang, X. Wang, D. LaMontagne, H. Wu, Z. Wang and Y. C. Cao, Self-Assembled Colloidal Superparticles from Nanorods, *Science*, 2012, **338**(6105), 358–363; (b) J. Zhuang, A. D. Shaller, J. Lynch, H. Wu, O. Chen, A. D. Q. Li and Y. C. Cao, Cylindrical Superparticles from Semiconductor Nanorods, *J. Am. Chem. Soc.*, 2009, **131**(17), 6084–6085.